Journal of Catalysis 286 (2012) 111–123

Contents lists available at SciVerse ScienceDirect

Journal of Catalysis

journal homepage: www.elsevier.com/locate/jcat

Chemical and structural effects of silica in iron-based Fischer–Tropsch synthesis catalysts

Haiyun Suo [a,c], Shengguang Wang [b], Chenghua Zhang [a,b,*], Jian Xu [b], Baoshan Wu [a,b], Yong Yang [a,b], Hongwei Xiang [a,b], Yong-Wang Li [a,b]

[a] State Key Laboratory of Coal Conversion, Institute of Coal Chemistry, Chinese Academy of Sciences, Taiyuan 030001, PR China
[b] National Engineering Laboratory for Indirect Coal Liquefaction, Institute of Coal Chemistry, Chinese Academy of Sciences, Taiyuan 030001, PR China
[c] Graduate University of Chinese Academy of Sciences, Beijing 10039, PR China

ARTICLE INFO

Article history:
Received 14 July 2011
Revised 26 September 2011
Accepted 22 October 2011
Available online 7 December 2011

Keywords:
Fischer–Tropsch synthesis
Fe/SiO_2 catalyst
$Fe–SiO_2$ interaction
Chemical effect
Structural effect

ABSTRACT

Fe/SiO_2 catalysts with different Fe/Si molar ratios were used to investigate the effects of silica on chemical/structural properties and Fischer–Tropsch synthesis (FTS) performance of iron-based catalysts. In the chemical aspect, silica interacts with Fe species by the formation of Fe—O—Si structure, which further transforms into an Fe_2SiO_4 phase during FTS reaction. The interaction largely disturbs the electronic structure of Fe atoms in iron oxide phases and in turn resists the reduction and activation of catalysts. In the structural aspect, silica increases the dispersion of Fe species and inhibits the aggregation of active iron particles. Addition of silica largely changes the adsorption sites of catalysts, i.e., decreases the number of weak H adsorption sites but improves the adsorption strengths of H, C, and O on reduced or carburized catalysts. With increasing amounts of silica, the chemical and structural effects cause the firstly decrease and then the increase of the initial FTS activity and the selectivities of heavy hydrocarbons and olefins during the Fischer–Tropsch synthesis. In addition, an important finding is that a proper amount of silica apparently suppresses the methane selectivity and stabilizes the iron carbide in the FTS reaction.

1. Introduction

Fischer–Tropsch synthesis (FTS) enables the production of virtually sulfur and aromatic free transportation fuels and chemical feedstock from alternative carbon sources to crude oil [1,2]. Iron-based catalysts are preferentially used in FTS processes because of their low cost, high FTS activity, feed flexibility ($H_2/CO = 0.5–2.5$), and wide temperature adaptability (230–350 °C) [3,4]. To improve the FTS performance, the addition of structural promoters or supports (SiO_2, Al_2O_3, and other support materials) into iron-based catalysts to suppress the agglomeration of active phases and to improve the mechanical properties of catalysts is beneficial [5–7].

SiO_2 has been extensively investigated as catalyst support/promoter [8–10]. The role of silica in FTS catalysts is generally considered to be physical in nature: providing large surface areas, stabilizing small metal crystallites, and enhancing the attrition resistance of catalysts [5]. However, addition of silica also suppresses the reduction of iron oxides and decreases the activity of catalysts, due to the strong interaction between iron and silica [6,11–14]. Wielers et al. [12] studied silica-supported iron catalysts and suggested that reduction of the Fe/SiO_2 catalyst proceeds via an iron (II) silicate phase that cannot be completely reduced to α-Fe at higher temperature. Dlamini et al. [13] investigated the effect of the incorporation order of SiO_2 on precipitated $Fe/Cu/K/SiO_2$ catalysts. They found that silica added either during or after precipitation hindered the reduction and carburization of the catalyst. The low extent of reduction and carburization observed with catalysts that contain precipitated SiO_2 resulted in low catalytic activity. Zhang et al. [14] investigated the reduction of co-precipitated Fe/SiO_2 catalyst and found the formation of an iron (II) silicate phase that largely inhibited the activation of iron oxides, and subsequently resulted in low activity. It should be noted that the effect of silica on the reduction of iron oxides is not due only to the formation of the barely reducible Fe—O—Si species or iron silicate phases. If only limited to the local interaction (Fe—O—Si) between iron and silica, part of the iron oxides in Fe/SiO_2 catalysts would show reduction behaviors similar to those of pure iron catalysts. Actually, a small amount of silica can shift reduction curves of Fe/SiO_2 catalysts to high temperatures in TPR characterizations [14]. Some remote interactions between iron and silica must exist, which influence the reduction of iron oxides. However, there is no report in the literature on remote interaction between iron and

* Corresponding author at: State Key Laboratory of Coal Conversion, Institute of Coal Chemistry, Chinese Academy of Sciences, P.O. Box 165, Taiyuan 030001, PR China. Fax: +86 351 7560668.
E-mail addresses: zhangchh@sxicc.ac.cn (C. Zhang), ywl@sxicc.ac.cn (Y.-W. Li).

0021-9517/$ - see front matter © 2011 Elsevier Inc. All rights reserved.
doi:10.1016/j.jcat.2011.10.024

silica. Besides, silica has apparent effects on FTS product selectivity [6,9,14–16]. Dry [9] studied the influence of different supports on the FTS performance of precipitated Fe–Cu catalysts and found that the SiO_2-supported precipitated iron catalyst had a much higher activity and wax selectivity than the precipitated iron catalysts supported with Al_2O_3, MgO, ZnO, or Cr_2O_3 or with no support. Bukur et al. [6] and Yang et al. [15] observed an unexpected hydrocarbon distribution shifting to higher-molecular-weight products in catalysts with more silica content (100Fe/5Cu/4.2 K/$x$$SiO_2$ and 100Fe/12Mn/1.5 K/$x$$SiO_2$). However, Wan et al. [16] and Zhang et al. [14] found that hydrocarbon distribution shifted to light hydrocarbons and methane in 100Fe/6Cu/5 K/25SiO_2 catalyst and 100Fe/25SiO_2 catalyst, respectively. It is apparent that the effects of silica on the product selectivity are inconsistent in the literature. The above studies were conducted under different conditions and over catalysts with multiple components [6,15–17]. Especially, when chemical promoters other than silica were added, these promoters may affect the FTS performance jointly with silica [17]. The other promoters also lead to a synergetic effect on the FTS reaction and hide the intrinsic role of silica in FTS iron catalysts. Although the Fe/SiO_2 catalysts for FTS have been extensively investigated, the effect of SiO_2 on iron-based catalysts is still elusive.

In the present work, a series of binary Fe/SiO_2 catalysts were designed and prepared by a co-precipitation method. These model catalysts were characterized by N_2 adsorption, H_2 temperature-programmed reduction (TPR), H_2 and CO temperature-programmed desorption (TPD), transmission electron microscopy (TEM), Fourier transform infrared spectroscopy (FT-IR), X-ray diffraction (XRD), Mössbauer effect spectroscopy (MES), and X-ray photoelectron spectroscopy (XPS). FTS performances of catalysts were evaluated in a fixed-bed reactor and correlated with the characterization results.

2. Experimental

2.1. Catalyst preparation

The Fe/SiO_2 catalysts were prepared via a co-precipitation method. The detailed preparation method has been described elsewhere [17]. In brief, mixture solutions containing Fe $(NO_3)_3$ (99.9%) and $Si(OC_2H_5)_4$ with an Fe/Si atomic ratio of 100/x (x = 0, 1, 5, 10, 15, 25, 50) were precipitated using an ammonium solution at 80 °C and pH 8.5–9.0. After precipitation, the precipitates were aged for 2 h and then washed and filtered. Then, the filtered cakes were dried overnight at 120 °C, followed by calcination for 5 h in air at 500 °C. The catalysts were denoted as FexSi (x = 0, 1, 5, 10, 15, 25, 50).

Additionally, three model samples were also prepared to study H_2 adsorption behaviors. A model sample named 5Fe100Si (5Fe/100Si, atomic ratio) and a pure SiO_2 sample were prepared using the same co-precipitation method. A model sample named Fe25SiM was prepared via a mechanical mixing method. In brief, mixture powders containing Fe_2O_3 and SiO_2 with Fe/Si atomic ratio 100/25 were subjected to vigorous mechanical agitation for 30 min.

2.2. Catalyst treatments and characterizations

The reduced catalyst samples used for XRD, TEM, and MES characterizations were prepared by reducing the fresh catalysts in a quartz tube with synthesis gas (H_2/CO = 2) at 300 °C and a gas space velocity (SV) of 1 NL/(g of catalyst·h) for 20 h. After reduction, the catalysts for MES and XRD measurements were coated with paraffin to prevent oxidation. The samples for TEM measurement were passivated with 1%O_2/99% N_2 at room temperature. After FTS reaction, the used catalysts were passivated by a flow of 1%O_2/99%N_2 at room temperature and then collected for XRD, TEM, and MES measurements.

The BET surface area, pore volume, and average pore diameter of the fresh catalysts were obtained via nitrogen physisorption in ASAP 2420 equipment (Micromeritics, USA). Each sample was degassed under vacuum at 90 °C for 1 h and 350 °C for 8 h prior to the measurement.

XRD patterns were obtained with a D/max-RA X-ray diffractometer (Rigaku, Japan) using Cu$K\alpha$ radiation (γ = 1.5406 Å) at 40 kV and 150 mA. A step scan mode was used with a scan rate of 0.02° (2θ) per second from 15° to 75°. The crystallite diameter was determined by substituting the half width of a chosen peak into the Debye–Scherrer equation.

MES experiments were carried out in an MR-351 constant-acceleration Mössbauer spectrometer (FAST, Germany) drive with a triangular reference signal at room temperature or −253 °C. The radioactive source was 25-mCi ^{57}Co in a Pd matrix. Data analysis was performed using a nonlinear least-squares fitting routine that modeled the spectra as a combination of singlets, quadruple doublets, and magnetic sextets based on a Lorentzian lineshape profile. The components were identified based on their isomer shift (IS), quadruple splitting (QS), and magnetic hyperfine fields (Hhf). Magnetic hyperfine fields were calibrated with the 330-kOe field of α-Fe at the ambient temperature.

The samples were examined with transmission electron microscopy (TEM) in JEM-2100 equipment (JEOS, Japan) operated at 200 kV. Samples were crushed and suspended in ethanol under ultrasonic vibration and finally dispersed on a holey carbon film on a copper grid.

The FT-IR spectra were recorded with a VERTEX 70 (Bruker, Germany) FT-IR spectrophotometer, equipped with a deuterium triglycine sulfate (DTGS) detector. Samples of 1–2 mg were mixed with 100 mg KBr and pressed into translucent disks at room temperature. All spectra were taken in the range 4000–400 cm^{-1} at a resolution of 4 cm^{-1}. The spectra of all samples were presented by subtracting the background spectrum.

XPS were recorded with a VG MiltiLab 2000 system (VG) at a base pressure of 1×10^{-9} mbar. Samples were excited with monochromatized Al$K\alpha$ radiation ($h\nu$ = 1486.6 eV). The analyzer was operated in a constant-pass energy mode (20 eV). The C1s peak of adventitious carbon (284.6 eV) was used as a reference for estimating the binding energy. The binding energies are given with an accuracy of ±0.1 eV.

H_2-TPR studies were carried out with Autochem II 2920 equipment (Micromeritics, USA). A sample of 40 mg of catalyst was loaded into a U-type quartz tube reactor and ramped from room temperature to 1000 °C in 10% H_2/90% Ar. The heating rate was maintained at 10 °C/min and the flow rate at 50 ml/min. The variation of the outlet gas concentration was monitored by a thermal conductivity detector (TCD). Isopropyl alcohol gel (−88 °C) was used to remove water formed during tests. In order to quantify the degree of reduction in H_2-TPR, amount of H_2 consumption during the reduction of CuO oxides under the same TPR procedures was used as a calibration standard for peak areas.

H_2-TPD studies were conducted in the same equipment as TPR. About 0.2 g of catalyst was placed in the reactor. The sample was reduced with pure H_2 (50 ml/min) at a temperature of 350 °C for 10 h. The catalyst was subsequently flushed at the same temperature with Ar gas (50 ml/min) for 30 min. After reduction, the sample was cooled to 50 °C, and then H_2 flow (50 ml/min) was continued for 30 min at 50 °C. After adsorption, the system was purged with Ar gas (50 ml/min) for 30 min to remove physisorbed H_2. The H_2-TPD profile was monitored using TCD while the temperature was increased from 50 to 800 °C at a rate of 10 °C/min.

CO-TPD experiments were performed in an atmospheric quartz tube flow reactor (5 mm i.d.). The outlet of the reactor was

connected to a quadruple mass spectrometer (Omnistar, Pfeiffer) through a capillary inlet system. In each CO-TPD experiment, 0.1 g of catalyst was loaded into the reactor and reduced with 5% CO/95% He (50 ml/min) at 300 °C for 12 h. After reduction, the sample was cooled to 50 °C with 5% CO/95% He (50 ml/min) and switched to high-purity He (50 ml/min) until the baseline of the CO signal leveled off. Finally, the temperature was increased to 800 °C at 10 °C/min. CO-TPD profiles were monitored by recording the mass signal of 28 in the outlet gas.

H_2-TPD profiles were fitted with Gaussian curves to quantify the amount of hydrogen species (see supporting information Fig. S1). H_2 uptake was determined by the area of TCD curves. Iron dispersion and particle size were calculated from the amount of H_2 chemisorbed onto metallic iron surfaces according to a method reported by Jones et al. [18].

2.3. Catalyst evaluation

The experiments were conducted in a 12-mm i.d. stainless steel fixed-bed reactor with an isothermal bed length of 5 cm. For all the experiments, 3 g of catalysts (40–60 mesh) was loaded into the reactor; the remaining volume of the reactor was filled with quartz granules (20–40 and 40–60 mesh). A detailed description of the reactor and product analysis systems has been given elsewhere [15,19]. In brief, the flow rates of the gases were controlled by mass flow meters separately (5850E, Brooks). The flow rate of the tail gas was measured by a wet-gas flow meter. All the catalysts were reduced with synthesis gas (H_2/CO = 2.0) at 300 °C and a gas space velocity (SV) of 1 NL/(g of catalyst·h) for 20 h; then, the reactor was cooled to 220 °C. Then, the system was regulated to 1.50 MPa, 2 NL/(g of catalyst·h), and the temperature was gradually increased to 280 °C at 10 °C /h. The tail gas was analyzed on line by gas chromatographs (GC) (Models 6890 N and 4890D, Agilent). The nongaseous products in the hot and cold traps were collected over 24 h for the calculation of mass balance and sampled for analysis.

3. Results and discussion

3.1. Physicochemical properties of catalysts

The BET surface area, pore volume, and average pore diameter of catalysts as prepared are shown in Table 1. It can be seen that the BET surface area of the silica-free catalyst (Fe0Si) is about 18 m^2/g. The silica addition apparently improves the BET surface area of catalysts. The surface areas increase from 18 to 222 m^2/g, while the average pore diameters decrease significantly with increasing silica content.

The FT-IR spectra of catalysts are shown in Fig. 1. In the spectrum of the Fe0Si catalyst, two broad bands around 538 and 465 cm^{-1} are present, both of which are characteristic bands of

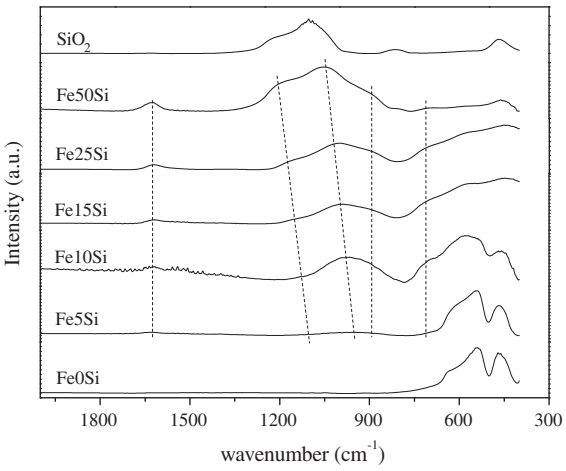

Fig. 1. FT-IR spectra of catalysts as-prepared.

Fe–O in the α-Fe_2O_3 phase [20]. With the incorporation of silica, new bands appeared at 1600, 1200–900, and 700 cm^{-1}. With further increasing silica content in catalysts, the characteristic Fe–O bands gradually weakened and widened, while the bands at 1200–900 cm^{-1} strengthened and shifted to high frequency. In contrast, the characteristic bands of silica appear at 1200, 1100, 800, and 460 cm^{-1}, which are attributed to the asymmetric Si–O–Si stretching vibration, the symmetric Si–O–Si stretching vibration, and the O–Si–O shearing vibration [21–23]. Apparently, substantial differences are apparent between spectra of silica or hematite (Fe0Si) and those of Fe/SiO_2 composite oxide catalysts. It has been known that iron oxyhydroxides were formed during precipitation, and a large percentage of Fe ions were at coordinate unsaturated sites, which may interact with SiO_2 to form Fe—O—Si complexes [24]. This kind of interaction between ferric ions and silica disturbs the Si–O–Si structure and leads to a red shift of the Si–O–Si stretching vibration [25]. In similar Fe/SiO_2 composite oxides, the bands around 1000 cm^{-1} were assigned to the asymmetric Fe—O—Si stretching vibration [21,22,25]. These results clearly proved that the Fe–SiO_2 interaction exists in the Fe/SiO_2 catalysts in a form of Fe—O—Si structure.

XPS was used to probe the Fe and Si electronic structures in catalysts. Fe2*p* XPS spectra (see Fig. S2 in the supporting information) indicate that Fe species are characteristic of trivalence in Fe_2O_3 [26]. There is no obvious difference in chemical shift in the Fe2*p* region. It is known that electrons in the outer Fe3*p* core level are more sensitive to the variation of electronic structures. Thus, the Fe3*p* XPS spectra were used to further probe the changes in electronic structure of Fe species in catalysts. The XPS spectra of Fe3*p* and Si2*p* are shown in Fig. 2. From Fig. 2a, it can be seen that the binding energies (BEs) of the Fe3*p* continually shift to high

Table 1
Textural properties of catalysts as-prepared and particle sizes of catalysts with different treatments.

Catalysts	BET surface area (m^2/g)	Pore volume (cm^3/g)	Average pore size (nm)	Average crystallite diameter (nm)		
				Fe_2O_3[a]	Fe_3O_4[b]	Fe_3O_4[c]
Fe0Si	18	0.17	32.2	39.7	22.4	34.7
Fe1Si	30	0.18	18.7	33.3	20.4	33.5
Fe5Si	78	0.31	12.5	16.9	14.2	17.1
Fe10Si	146	0.37	7.7	7.5	9.9	11.1
Fe15Si	187	0.31	5.0	5.9	NA[d]	NA[d]
Fe25Si	222	0.30	4.2	NA[d]	NA[d]	NA[d]

[a] Determined by XRD using Fe_2O_3 characteristic peak at 35.7° for as-prepared catalysts.
[b] Determined by XRD using Fe_3O_4 characteristic peak at 35.5° for catalysts after activation (300 °C, H_2/CO = 2.0, and 20 h).
[c] Determined by XRD using Fe_3O_4 characteristic peak at 35.5° for catalysts after reaction (280 °C, 1.5 MPa, H_2/CO = 2.0, and 200 h).
[d] Not available.

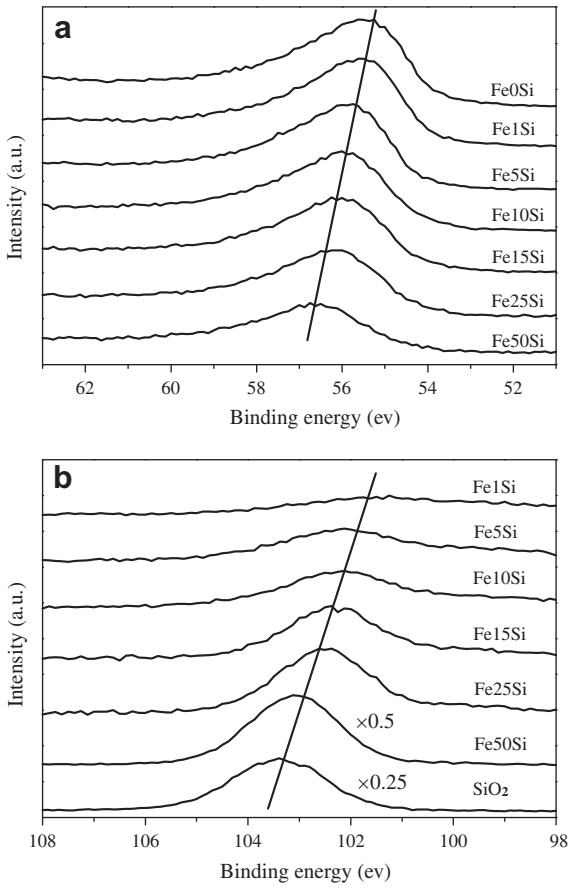

Fig. 2. XPS spectra of catalysts as-prepared: (a) Fe3*p* spectra of catalysts; (b) Si2*p* spectra of catalysts.

values with increasing silica content. At the same time, Si2*p* BEs (Fig. 2b) shift to lower values with increasing iron content in these samples. The chemical shifts reflect changes in the electronic structures of corresponding elements in the samples [27]. For example, if bonding to silica transferred an electron to the Fe species, the Fe BE would shift to lower energy, and if bonding to silica transferred an electron from the Fe species, the Fe BE would shift to higher energy. From this point of view, it is apparent that there is electron transfer from Fe to Si atoms, showing an electron-deficient state of Fe species in Fe/SiO_2 catalysts. Considering the continuity of BE shifting for all the spectra, the electron transference is a long-range phenomenon instead of localizing in the near neighbor of Si species. The electron transference was also observed in similar Fe/SiO_2–ZrO_2 and FeMo catalysts [25,28].

3.2. Crystallite structure and morphology of catalysts

XRD was used to characterize the iron-phase structure of catalysts. XRD patterns of catalysts as-prepared, activated, and after reaction are shown in Fig. 3a–c, respectively. For as-prepared catalysts (Fig. 3a), the XRD pattern of Fe0Si exhibits the characteristic diffraction peaks of hematite (α-Fe_2O_3). With increasing silica content, the diffraction peaks of hematite become broad and even vanish. In XRD patterns of activated catalysts (Fig. 3b), the observed iron phases are mainly magnetite (diffraction peaks at 30.1°, 35.5°, 37.1°, 43.1°, 57.0°, and 62.6°) and iron carbide (39.3°, 43.5°, and 44.1°). Similarly, these characteristic peaks gradually decrease in intensity with the incorporation of silica. After FTS reactions, XRD patterns still exhibit the characteristic peaks of magnetite and carbide (Fig. 3c). Additionally, the XRD pattern of

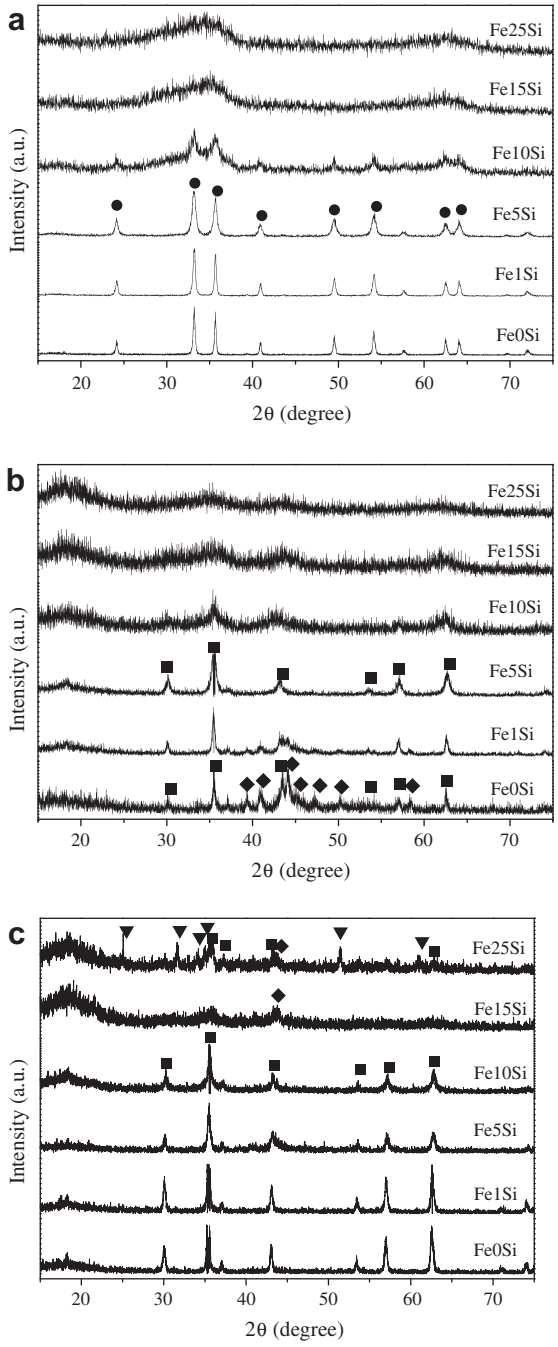

Fig. 3. XRD patterns of catalysts: (a) as-prepared; (b) after activation (300 °C, H_2/CO = 2.0, and 20 h); (c) after reaction (280 °C, 1.5 MPa, H_2/CO = 2.0, and 200 h). Circles (●): hematite; square (■): magnetite; diamond (♦): carbide; triangle (▼): fayalite.

Fe25Si also shows the characteristic peaks of Fe_2SiO_4 (JCPDS 76-0512), further confirming the existence of the Fe—O—Si structure.

MES was used to determine the iron-phase composition of catalysts after activation and reaction. The spectra (see Figs. S3 and S4 in the supporting information) exhibited complex magnetic interactions due to the presence of multiple magnetic phases. MES parameters of various phases and their relative contributions to spectral absorption areas are tabulated in Table 2. Percentage areas can be translated to percent content of the various iron phases, assuming similar Mössbauer efficiency (recoil-free fraction) for all phases. As shown in Table 2, the MES line of each sample is the result of the superposition of at least five subspectra associated

Table 2
MES[a] parameters and compositions of iron phases in catalysts after activation[b] and reaction.[c]

Catalysts	Phases	MES parameters and compositions[d]		Carbide difference (%)
		After activation	After reaction	
Fe0Si	Fe_3O_4	0.50/−0.06/506/17.4 0.56/−0.05/456/8.3	0.29/−0.04/506/37.3 0.59/−0.02/509/25.2 0.82/−0.04/483/35.2	−72
	χ-Fe_5C_2	0.32/0.08/247/36.8 0.34/−0.06/215/27.9 0.20/0.02/121/9.6	0.30/0.03/245/1.2 0.30/0.02/207/1.1	
Fe1Si	Fe_3O_4	0.48/−0.07/509/36.8 0.60/0.06/463/9.9	0.28/−0.07/510/30.0 0.62/−0.05/513/39.7 0.80/−0.05/476/26.5	−49.5
	χ-Fe_5C_2	0.35/0.10/248/27.2 0.32/−0.01/214/20.1 0.24/−0.01/120/6.0	0.30/0.02/247/1.0 0.30/0.03/203/2.8	
Fe5Si	Fe_3O_4	0.36/−0.02/501/44.9 0.65/−0.05/469/38.4	0.25/0.08/502/24.0 0.55/0.00/505/47.9 0.77/−0.07/470/25.8	−14.4
	χ-Fe_5C_2	0.34/0.06/250/6.8 0.25/0.15/208/4.1 0.28/0.00/120/5.8	0.30/0.01/246/1.3 0.30/0.00/204/1.0	
Fe10Si	Fe_3O_4	0.50/−0.04/506/47.1 0.63/−0.07/460/32.7	0.29/−0.09/503/30.2 0.66/−0.06/504/40.2 0.49/0.00/457/18.9	−9.5
	χ-Fe_5C_2	0.33/0.02/248/12.9 0.32/0.00/207/4.5 0.32/0.09/128/2.8	0.29/−0.01/245/6.5 0.31/0.00/203/4.2	
Fe15Si	Fe_3O_4	0.37/−0.07/497/20.5 0.67/0.09/497/16.8 0.45/−0.02/450/39.2	0.24/0.00/499/13.2 0.61/0.02/501/19.1 0.46/0.00/453/30.4	15.7
	χ-Fe_5C_2	0.37/0.00/244/13.9 0.32/−0.02/206/5.6 0.33/0.05/125/2.1	0.34/0.06/245/24.5 0.30/0.00/207/7.6 0.38/0.01/111/5.2	
Fe25Si	Fe_3O_4	0.36/−0.04/494/15.9 0.65/0.05/496/9.1 0.45/−0.04/451/59.2	0.36/−0.03/502/16.0 0.65/0.01/497/10.7 0.47/0.02/455/21.1 0.67/0.02/338/12.0	12.1
	χ-Fe_5C_2	0.37/0.09/255/4.6 0.36/−0.01/210/10.4 0.30/0.02/115/0.8	0.32/0.13/240/13.9 0.29/0.04/203/5.4 0.35/0.35/117/7.6	
	Fe_2SiO_4		1.33/2.93/110/13.3	

[a] The Mössbauer spectra of catalysts were obtained at −253 °C.
[b] Reduction conditions: 300 °C, H_2/CO = 2.0, 20 h, and 1 NL/(g of catalyst·h).
[c] Reaction conditions: 280 °C, 1.5 MPa, H_2/CO = 2.0, 2 NL/(g of catalyst·h), and TOS ca. 200 h.
[d] IS (mm/s)/QS (mm/s)/Hhf (kOe)/atomic percentage (%) for corresponding iron phases in catalysts.

with different iron sites in the sample. The subspectra with Hhf in the range 490–520 kOe are contributed to the Fe^{3+} sites, while those with Hhf in the range 300–480 kOe are contributed to the Fe^{2+} sites of ferrimagnetic Fe_3O_4 phases [29,30]. The subspectra with 0.20 mm/s < IS < 0.40 mm/s and 110 kOe < Hhf < 250 kOe correspond to the three different sites of stoichiometric iron carbide (χ-Fe_5C_2) [31,32]. The subspectrum with IS = 1.33 mm/s and QS = 2.93 mm/s is associated with crystalline fayalite (Fe_2SiO_4) [33]. After activation treatments, the predominant phase of the silica-free catalyst (Fe0Si) is χ-Fe_5C_2 (74.3%), and the remainder is Fe_3O_4. With the addition of a small amount of silica (Fe1Si and Fe5Si), the content of χ-Fe_5C_2 decreases, while that of Fe_3O_4 increases sharply. With a further increase in silica content (Fe10Si, Fe15Si, and Fe25Si), the amount of χ-Fe_5C_2 species is kept at about 20%. On the whole, silica addition inhibits the formation of χ-Fe_5C_2 catalysts during the activation. After FTS reactions, iron carbide content in low-silica-promoted catalysts is greatly decreased, while it further increases in high-silica-promoted catalysts. The decrease in the content of iron carbides is probably reoxidized by the vapor produced in FTS reactions [34,35]. Table 2 also lists the difference in the content of iron carbides between activation and FTS reaction. Clearly, the reoxidation extent of iron carbides is inhibited by silica. A similar stabilizing effect of silica on iron carbide was also reported by Sirimanothan et al. [36]. In Fe25Si catalyst, the Fe_2SiO_4 phase was also detected by MES after reaction, which is in agreement with the XRD results.

The XRD results indicate that the crystallinity of iron phases becomes poor with the incorporation of silica. It seems that silica disturbs the iron phase structure or segmentalizes iron oxide/carbide phases into small particles. The average crystallite diameters of iron oxide phases in catalysts after different treatments, determined by XRD, are listed in Table 1. It can be found that the average crystallite diameter of iron oxides decreases continually with increasing silica content, irrespective of the sample treatment

conditions. Compared to the as-prepared samples, the iron oxide particles in the low-silica-promoted samples become shrunken after activations, while their sizes increase slightly after reactions. For the high-silica-promoted samples, the iron oxide particle sizes are undetermined, due to the low XRD signal-to-noise ratios. TEM was used to compare the particle distributions of low- and high-silica-promoted catalysts (Fe5Si and Fe25Si) with different treatments. TEM images (Fig. 4a) show that, in the case of Fe5Si, 75% of iron particles fall in the range of 8–25 nm with the most abundant particles having a diameter of 18.5 nm for the as-prepared sample. After activation in syngas at 300 °C for 20 h, the most abundant particles shift to about 15.5 nm diameter (Fig. 4b). After reaction under FTS conditions for 200 h (Fig. 4c), the iron particles grow slightly, with the most abundant particles at diameter 19.5 nm. These results are in good agreement with XRD results. In comparison, the image (Fig. 5) of Fe25Si shows much smaller iron particles with the most abundant at diameter 4.5 nm. In addition, the iron particles in the Fe25Si catalyst are very similar in size with different treatments. Even after FTS reactions, the iron particles grow only slightly, and about 95% of particles fall in the range 2–10 nm. These results indicate that the agglomeration of iron particles during FTS reactions can be effectively inhibited by the incorporation of enough silica.

3.3. Reduction behavior of catalysts

The reduction behavior of catalysts was studied by H_2-TPR (Fig. 6). The corresponding H_2 consumptions are listed in Table 3. As shown in the figure, the profile of Fe0Si shows two well-separated H_2 consumption peaks at about 377 and 589 °C. With the addition of silica, TPR profiles become complicated. First, the reduction peaks shift to higher temperatures for Fe1Si and Fe5Si catalysts. In contrast, the first peaks become broad, and the second peaks gradually shift to lower temperatures for Fe10Si, Fe15Si, and Fe25Si catalysts. Second, H_2 consumption for the first peaks is increased to the theoretical value of Fe_2O_3 reduction to a nonstoichiometric iron oxide phase (Fe_xO, $0.84 < x < 0.95$). In contrast, the H_2 consumptions for the second peaks continuously decrease. Third, a new reduction peak occurs at about 900 °C in these high-silica-content catalysts. The H_2 consumption for this peak increases with increasing silica content. At last, the total hydrogen consumption of Fe25Si (1.37 mol H_2/mol Fe) is apparently lower than the theoretical value for the reduction of Fe_2O_3 to α-Fe (1.5 mol H_2/mol Fe). This result implies that this catalyst is not completely reduced in H_2 atmosphere below 1000 °C.

H_2-TPR results show that the silica addition has complex effects on the reduction behavior of iron oxides in catalysts. First, a small

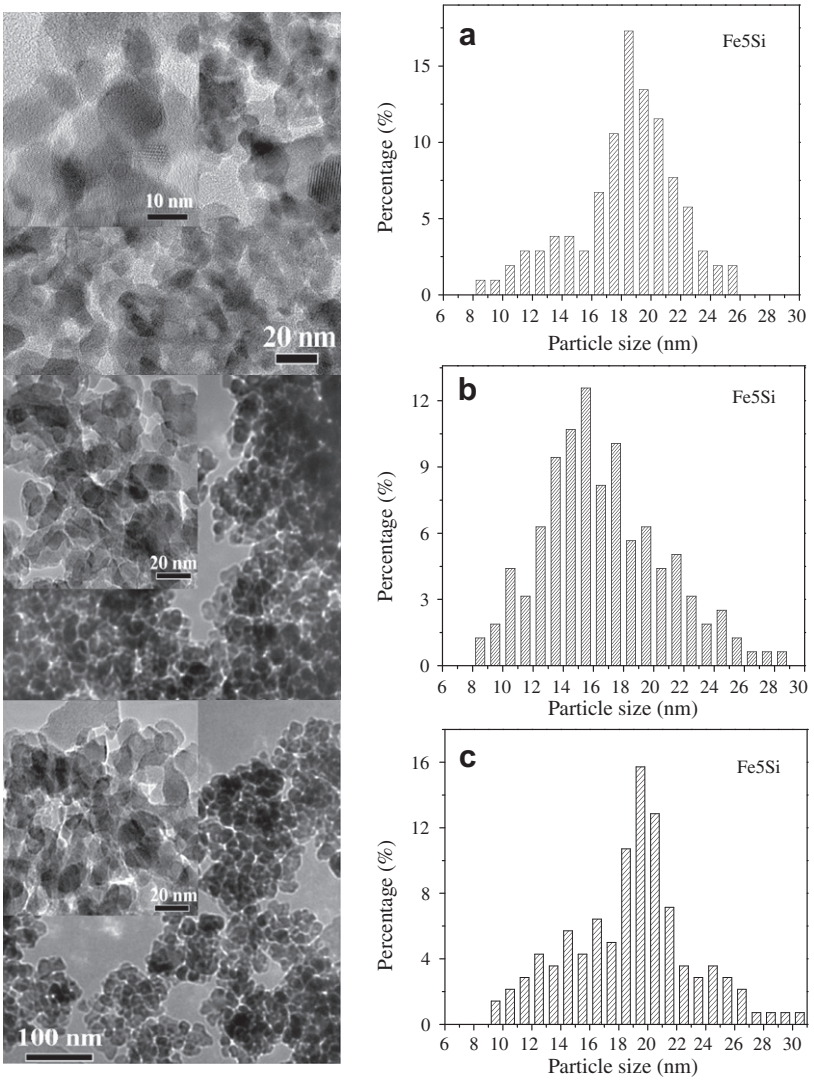

Fig. 4. TEM images and particle size distributions of Fe5Si with different treatments: (a) as-prepared; (b) after activation (300 °C, $H_2/CO = 2.0$, and 20 h); (c) after reaction (280 °C, 1.5 MPa, $H_2/CO = 2.0$, and 200 h).

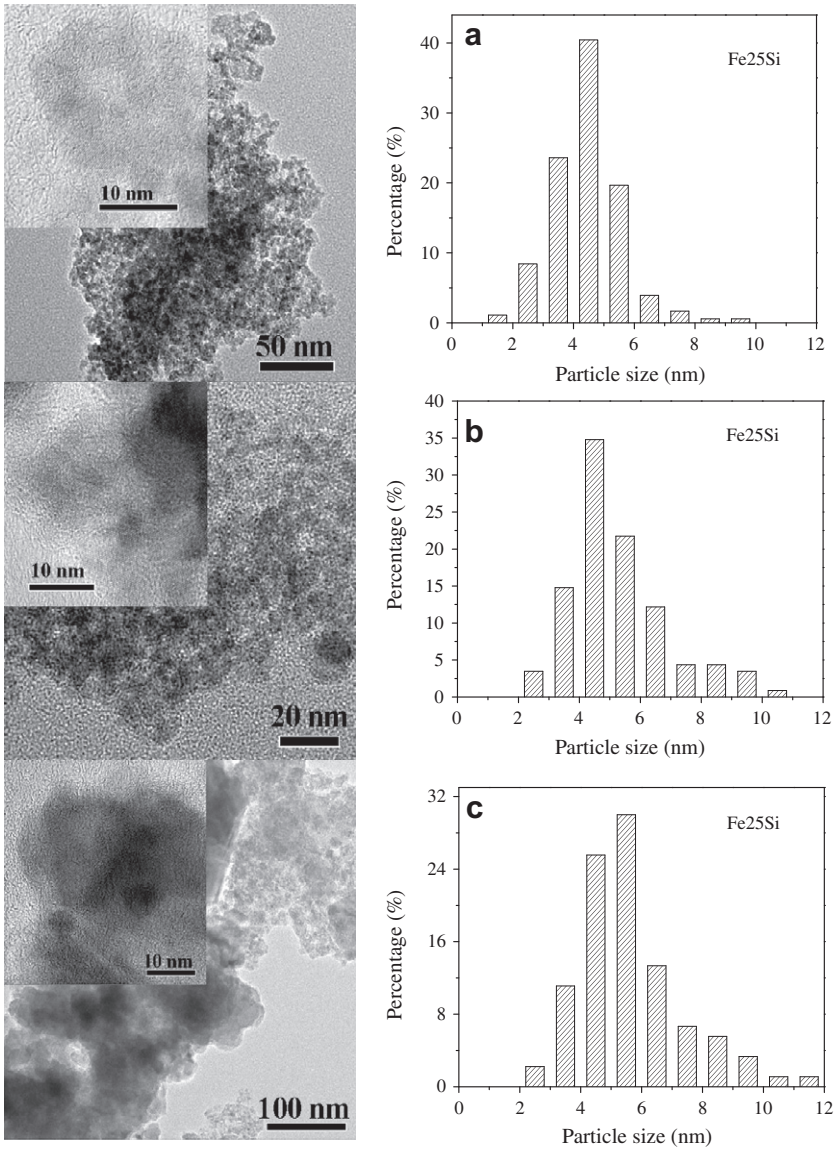

Fig. 5. TEM images and particle size distributions of Fe25Si with different treatments: (a) as-prepared; (b) after activation (300 °C, H_2/CO = 2.0, and 20 h); (c) after reaction (280 °C, 1.5 MPa, H_2/CO = 2.0, and 200 h).

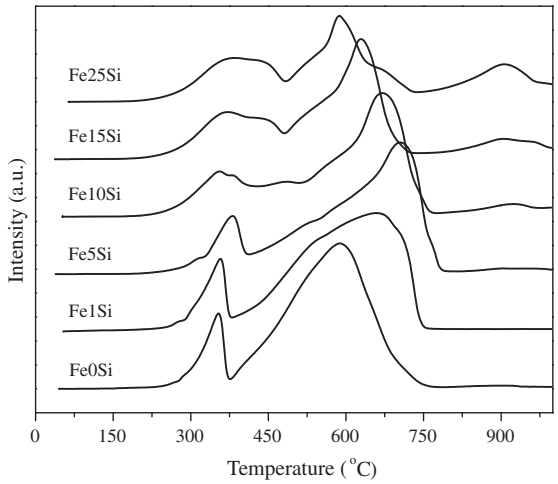

Fig. 6. H_2 TPR profiles of catalysts.

amount of silica addition inhibits the reduction of iron oxides. This inhibitive effect is not due to the barely reducible Fe—O—Si species or iron silicates, as observed in FT-IR and XRD characterizations. Such a small amount of silica is not enough to interact directly with all iron atoms to form Fe—O—Si covalent bonds. It probably results from the variation of electronic structures of Fe atoms, which has been proven by XPS results. The effect of silica on the electronic properties of Fe atoms is remote but not local, which leads to an electron-deficient state of all Fe species in silica-promoted catalysts relative to the silica-free catalyst. The electron-deficient state means that more core-level electron density of Fe nuclei takes part in Fe–O covalent bonds [28]. Thus, the Fe–O bonds are strengthened and became difficult to cleave during the reduction. Second, a large amount of silica at least improves the reduction of partial Fe species. As displayed in the above XRD results, the crystallite size of iron oxides is decreased by silica. Iron oxides with small particle sizes have a larger percentage of surface atoms than of bulk iron oxides. Obviously, surface atoms have a higher probability of contact with H_2 during the reduction. Therefore, the reduction of iron oxides is abnormally improved by a large amount of

Table 3
Quantitative results of H_2 consumption in H_2 TPR process.

Catalyst	Peak		H_2 consumption (mol H_2/mol Fe)	Assignment	Total H_2 consumption (mol H_2/mol Fe)
	Serial	T (°C)			
Fe0Si	1st	354	0.17	$Fe_2O_3 \rightarrow Fe_3O_4$	1.49
	2nd	589	1.32	$Fe_3O_4 \rightarrow Fe$	
Fe1Si	1st	357	0.17	$Fe_2O_3 \rightarrow Fe_3O_4$	1.48
	2nd	570–680	1.31	$Fe_3O_4 \rightarrow Fe$	
Fe5Si	1st	381	0.17	$Fe_2O_3 \rightarrow Fe_3O_4$	1.45
	2nd	705	1.28	$Fe_3O_4 \rightarrow Fe$	
Fe10Si	1st	350–470	0.41	$Fe_2O_3 \rightarrow Fe_xO$ or Fe^{2+}	1.46
	2nd	590–680	0.93	$Fe_xO \rightarrow Fe$	
	3rd	924	0.12	$Fe^{2+} \rightarrow Fe^0$	
Fe15Si	1st	350–450	0.45	$Fe_2O_3 \rightarrow Fe_xO$ or Fe^{2+}	1.44
	2nd	628	0.74	$Fe_xO \rightarrow Fe$	
	3rd	918	0.25	$Fe^{2+} \rightarrow Fe^0$	
Fe25Si	1st	350–440	0.46	$Fe_2O_3 \rightarrow Fe_xO$ or Fe^{2+}	1.37
	2nd	588	0.54	$Fe_xO \rightarrow Fe$	
	3rd	906	0.37	$Fe^{2+} \rightarrow Fe^0$	

silica. Furthermore, Fe_xO is stabilized as the intermediate phase during the reduction process. Fe_xO is thermodynamically unstable in bulk, while its structure can be stabilized by the large contribution of surface energy in nanoscale materials [30]. This is also in accord with the nanosize of iron oxides in high-silica-content catalysts. Third, besides the electronic and dispersion effects, silica interacts strongly with its neighbor Fe atoms, which forms hardly reducible Fe—O—Si species [37]. These species have been verified by FT-IR, XRD, and MES in as-prepared, activated, and reaction samples. H_2 TPR further confirms the strong Fe–SiO_2 interaction. For example, a high-temperature peak at about 900 °C appears in H_2 TPR curves of silica-promoted catalysts. The intensity of this peak is dependent on the silica content, implying that the peak is attributed to the reduction of a specific Fe species interacting with silica.

3.4. H_2 chemisorption

H_2-TPD is used to investigate the effect of SiO_2 on the H_2 adsorption behavior of iron catalysts (Fig. 7). H_2 desorption over silica-promoted catalysts mainly occurs in two broad temperature ranges: below 300 °C and above 300 °C. For Fe0Si and Fe1Si, hydrogen desorption is only observed below 300 °C: a sharp peak at ca. 70–100 °C and a broad tail at 120–300 °C. In the case of Fe5Si, the profile of H_2 desorption below 300 °C is similar to that of Fe0Si, while a small peak appears at ca. 615 °C. With a further increase of silica content, four evident desorption peaks appear in H_2-TPD curves: a peak at ca. 100 °C, a broad peak at 150–300 °C, a broad peak at ca. 430 °C, and a sharp peak at 530–630 °C. With increasing silica content, the intensity of the first peak at ca. 100 °C first increases, passes a maximum at an Si/Fe ratio of 5/100, and then decreases gradually. However, other peaks show a monotonic increase in their intensities. In addition, the peaks below 300 °C shift to higher temperatures and become broader, indicating that the hydrogen adsorption sites become more uneven with increasing silica content.

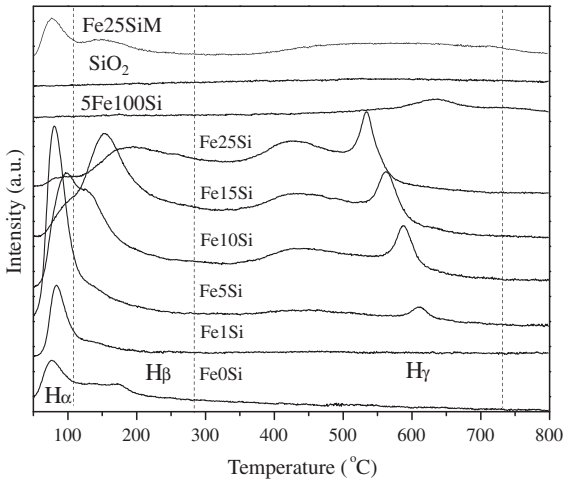

Fig. 7. H_2 TPD profiles of catalysts.

Due to the heterogeneity of catalysts, it is difficult to directly identify the surface hydrogen adsorption sites in these silica-containing catalysts. However, we can distinguish these surface adsorption sites through comparing model and literature results with the present study. As proved earlier, the Fe–SiO_2 interaction affects the reduction of iron oxides and would lead to different iron species (iron oxide, iron silicate, and metallic iron) in catalysts. MES was used to determine the iron-phase compositions of catalyst samples used in H_2 TPD (see Table S1 and Fig. S5 in the supporting information). As shown in the MES results, the iron oxides of Fe0Si and Fe1Si catalysts can be completely reduced to metallic iron, whereas other catalysts contain iron oxides and/or iron silicates besides metallic iron with the same pretreatment process in H_2-TPD experiments. Therefore, H_2-TPD peaks of Fe0Si and Fe1Si catalysts can be attributed to hydrogen desorption from metallic iron surfaces. Previous studies [38–45] demonstrated that hydrogen desorption usually occurs below 300 °C on single-crystal iron planes or polycrystalline iron surfaces, which are similar to the low-temperature desorption peaks in the present catalysts. From these works, hydrogen adsorbed onto low-index iron planes (110, 100, and 111) usually desorbs at temperatures below 200 °C depending on coverage [38–40]. However, on polycrystalline iron films/powders and the present catalysts, desorption peaks occur in the temperature range 200–300 °C, besides those below 200 °C [41,42]. Differently from single crystalline iron planes, real catalysts contain hundreds of iron particles with various geometric shapes and sizes. They expose not only low-index facets but also high-index faces and various defect sites due to the surface heterogeneity. Surface structural differences could lead to the different H_2-TPD profiles of the present catalysts from those of single crystalline iron planes. Moreover, it is well known that hydrogen adsorption over iron surfaces is stable at deep hollow or defect sites but relatively weak at shallow hollow or on-top sites

[43–45]. The H species desorbed at lower temperature (below 200 °C) imply a weak Fe–H bond strength. Thus, these hydrogen species are likely to occupy the shallow hollow, on-top, or weak adsorption sites, designated H_α. Correspondingly, the hydrogen species desorbed in the temperature range 200–300 °C could be ascribed to hydrogen adsorbed on the deep hollow or defect sites of metallic iron surfaces, designated H_β.

H_2-TPD profiles in high-temperature regions (above 300 °C), designated H_γ, are quite different from those on metallic iron surfaces [38–42]. It is evident that these peaks are not resulted from desorption of hydrogen on metallic iron sites. In supported metal catalysts [46,47], H_2 desorption peaks in higher-temperature regions were also observed, which were attributed to H_2 spilt over from very strong chemisorption sites on the support. For comparison, TPD curves of pure SiO_2, 5Fe100Si, and Fe25SiM samples are also shown in Fig. 7. No hydrogen desorption is detected over the pure SiO_2 sample under the same experimental conditions. The 5Fe100Si model sample only exhibits a small peak at 630 °C, which is quite similar to the hydrogen desorption peak at high temperature over the Fe5Si catalyst. In this sample, iron oxides are difficult to reduce to metallic iron due to the strong interaction between iron and silica. As confirmed in MES results, the high-silica-content catalysts are also composed of hardly reducible bivalent Fe species under the TPD pretreatment condition. Therefore, hydrogen species in higher-temperature regions are probably attributable to hydrogen chemisorbed on iron atoms of iron oxides or iron silicate compounds in catalysts. In the case of Fe25SiM, the profile of H_2 desorption below 300 °C is similar to that of Fe0Si catalyst, while a small and broad peak appears at 400–700 °C (Fig. 7 or Fig. S6 in the supporting information). Since the strong interaction between iron and silica is difficult to form after mechanical mixing, the high-temperature peak is probably due to H species that spilt over from SiO_2. It should be noted that the high-temperature peak in Fe25SiM is quite different from other catalysts. Thus, the H chemisorbed on iron atoms of iron oxides or iron silicates should not be overlooked on those co-precipitated Fe/SiO_2 catalysts. All in all, H_γ species may be attributed to hydrogen chemisorbed onto iron oxides and silicates or spilt over from SiO_2.

SiO_2 addition has evident effects on the H_2 adsorption on different iron sites. To quantitatively analyze the amount of corresponding hydrogen species, the H_2-TPD profiles were fitted with Gaussian curves to yield several peaks (see Fig. S1 in the supporting information), and the corresponding peak areas are listed in Table 4. As shown in Table 4, H_α species show a parabolic tendency, while H_β and H_γ species show increasing tendencies with increasing silica content over these catalysts. These variations could be caused by either the increased dispersion extent or the decreased reduction extent with the addition of silica. Therefore, H_2 uptakes are corrected by the reduction extent, i.e., based on a unit mass of metallic iron, to obviate the effect of reduction extent. From this point of view, H_α adsorption sites on metallic iron surfaces still show a parabolic tendency with increasing silica content. In contrast, H_β adsorption sites show monotonously increasing tendencies. These results indicate that H_α species are first increased with increasing iron dispersion but inhibited at high dispersion. In contrast, H_β species are increased by improving iron dispersion. The dispersion and the average crystallite diameter of iron particle can be calculated from the amount of H_α and H_β, which are also shown in Table 4. It is evident that the dispersion of iron increases monotonically with the silica content in catalysts. The average iron crystallite diameter show a monotonically decreasing tendency, which is in good agreement with XRD and TEM results.

3.5. CO chemisorption

CO-TPD was used to measure the CO adsorption behavior on carburized catalysts (Fig. 8). As can be seen, the main CO desorption peaks of all catalysts are located in the temperature range 300–650 °C. Actually, a very weak peak below 100 °C has also been detected on catalysts. As reported in the literature [48,49], desorption temperatures of molecular CO states on Fe single-crystal planes are below 200 °C, while the dissociative CO desorbs at about 500 °C. The CO-TPD curves on carburized iron catalysts were different from those on iron single-crystal facets. The temperatures of the main CO desorption peaks on the present catalysts are far higher than those of the molecular CO on the single-crystal iron surface and fall in the temperature range of dissociative CO desorption. Therefore, these CO desorption peaks at temperatures of 300–650 °C could be ascribed to the recombination of surface-adsorbed carbon species and oxygen atoms. As shown in Fig. 8, there are two desorption peaks observed on catalysts. Apparently, the first peak shifts to 343 °C once SiO_2 is incorporated and continues to about 390 °C with further increasing silica content. The second peak first shifts to higher temperatures, passes through a maximum temperature at Fe5Si, and then shifts to lower ones with increasing silica content. In Fe15Si and Fe25Si samples, two CO desorption peaks nearly overlap each other, demonstrating a small shoulder peak at about 390 °C and a more intense peak at around 430–450 °C.

In CO-TPD studies, catalyst samples contain the mixture of iron oxide and carbide phases under the applied pretreatment conditions. Therefore, CO-TPD can be regarded as a temperature-programmed redox reaction of carbon and oxygen species in catalysts. These carbon and oxygen species include not only the surface-adsorbed C and O species but also those in the crystal lattices of iron carbides and iron oxides. It is conceivable that surface-adsorbed C and O atoms are relatively easy to recombine into CO molecules, which would desorb at relatively low temperatures. However, the recombination of C and O in crystal lattices of iron

Table 4
Reduction extents, H_2 uptakes, dispersions, and average iron crystallite diameters for catalysts.

Catalysts	Reduction extent (%)[a]	H_2 uptakes (μmol/g)[b]					Dispersion (%)	Average iron crystallite diameter (nm)[d]
		H_α	H_α[c]	H_β	H_β[c]	H_γ		
Fe0Si	100.0	73.3	104.7	16.3	23.3		1.4	85.7
Fe1Si	100.0	87.4	125.8	12.0	17.3		1.6	76.7
Fe5Si	95.0	239.6	373.6	68.1	106.2	91.4	5.4	22.9
Fe10Si	75.0	322.3	660.0	88.9	182.1	345.2	9.4	13.0
Fe15Si	67.2	187.6	443.7	213.6	505.2	394.6	10.6	11.6
Fe25Si	33.1	39.0	199.9	194.5	996.8	363.4	13.4	9.2

[a] Catalysts were reduced in pure H_2 at 350 °C for 10 h. The reduction extents of catalysts were measured by MES.
[b] H_2 uptakes were obtained by integral of the corresponding peak based on unit mass of catalyst mass.
[c] H_2 uptakes were corrected by the iron content and the reduction extent, i.e., based on unit mass of metallic iron.
[d] Determined by H_2 uptake on metallic iron.

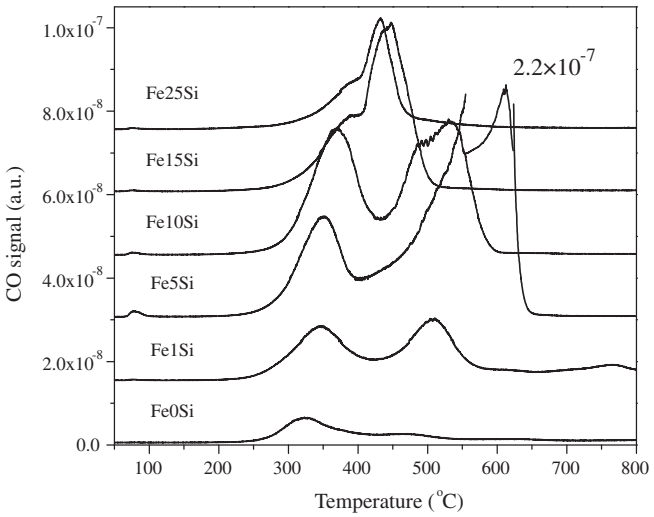

Fig. 8. CO TPD profiles of catalysts.

carbides and iron oxides would at least require overcoming additional migration barriers from bulks to surfaces. Desorption of bulk C and O species would require higher temperatures in the CO TPD process. Therefore, the lower-temperature peak (below 450 °C) could be attributed to desorption of surface and/or near-surface C and O species. Correspondingly, the higher-temperature peak may result from the reaction of bulk iron carbides with neighboring iron oxides. It should be noted that, in Fe15Si and Fe25Si catalysts, the high-temperature peaks largely shift to lower temperatures, showing overlapping peaks in the temperature range of surface C and O desorption (below 450 °C). This is in accord with the small iron particle size in these catalysts. The proportion of surface atoms would sharply increase at such small sizes. There is no obvious difference between surface and bulk in such small iron nanoparticles (2–8 nm). In addition, the desorption temperature of surface CO species continuously increases with increasing silica content. The results indicate that surface C and O adsorption or surface Fe–C and Fe–O bonds are strengthened by silica incorporation. It should be noted that H_2 and CO are co-adsorbed on working catalyst surfaces under FTS reaction conditions. H_2 preadsorption has an apparent influences on CO adsorption onto iron surfaces [40,50–53]. Thus, H_2 and CO co-adsorption behavior was studied using the TPD method over carburized catalysts (see Fig. S7 in the supporting information). It can be found that CO adsorption with H_2 co-presence follows the same trend as that without H_2 presence with regard to the effect of silica on C and O adsorption strengths.

3.6. FTS performance

3.6.1. Activity and stability

The effects of SiO_2 addition on the FTS performances of iron-based catalysts are presented in Table 5 and Fig. 9. Under a fixed set of process conditions, the CO conversion was used as a measure of FTS activity; i.e., higher conversion implies higher catalyst activity. The variation of the activity with time on stream (TOS) can be used as an indicator of catalyst stability. It can be found that the initial CO conversion of Fe0Si is the highest among all catalysts. However, its stability is very poor. The CO conversion quickly decreases from 77% at the beginning of the reaction to about 40% at a TOS of 96 h and is stable at this level in the subsequent reaction. With the addition of a small amount of silica, the reaction behavior of Fe1Si is somewhat similar to that of Fe0Si catalyst, while its steady CO conversion is quickly stabilized at a relatively high level. With further increasing silica content, the deactivation of the catalyst was not observed. The CO conversion first decreases, passes through a minimum at Fe10Si, and then sharply increases to a high level. These qualitative conclusions are confirmed by the specific activities in the form of CO turnover frequencies (TOFs; i.e., numbers of CO molecules converted per adsorption site per s) and CO space–time-yields (STYs; i.e., amounts of CO converted per g iron per h). Evidently, the initial specific activity quickly decreases, passes through a minimum at Fe10Si, and then slightly increases with increasing silica content in catalysts. The steady-state activity shows a similar changing tendency except for a slight changing extent. Bukur et al. [6] found that the FTS activity monotonically decreases with increasing SiO_2 content in 100Fe/5Cu/4.2 K/$x$$SiO_2$ (x = 0, 8, 24, 100) catalysts. In this study, the K_2SiO_3 solution as the SiO_2 precursor was added into undried and reslurried Fe/Cu precipitate. Complex interactions among Fe–SiO_2 and K–SiO_2 are inevitable. The authors attributed the decreased activity with increasing silica content to a lower degree of reduction and a reduction in the effective potassium content of the catalyst. Egiebor and Cooper [8] found that the steady-state CO conversion on 100Fe_2O_3/5.6CuO/3.6K_2O/$x$$SiO_2$ (x = 15, 35, 50) catalysts exhibits a slight increasing trend with increasing silica content. In this study, silica gel (200 mesh) was added to the nitrate solution before precipitation. Silica does not form a strong interaction with

Table 5
Activities and hydrocarbon selectivities of catalysts.[a]

Catalysts	Fe0Si		Fe1Si		Fe5Si		Fe10Si		Fe15Si		Fe25Si	
TOS (h)	24	192	24	192	24	192	24	192	24	192	24	192
CO conversion (%)	76.6	40.8	65.9	45.4	34.7	41.9	26.7	34.0	51.4	55.0	46.7	53.4
H2 conversion (%)	41.1	33.1	42.4	33.9	29.8	34.7	27.6	29.3	42.4	45.5	41.4	43.9
TOF × 10^3 (s^{-1})[b]	73.9	39.3	54.5	37.6	9.0	11.0	2.8	3.6	5.2	5.8	6.6	7.3
CO conversion rate (mmol/g-Fe/h)	34.1	18.1	28.2	19.5	15.3	18.4	12.1	15.4	23.8	26.6	24.1	26.9
H_2/CO exit ratio	4.73	2.13	3.44	2.38	2.30	2.41	2.08	2.17	2.50	2.39	2.17	2.36
CO_2 selectivity (mol%)	42.7	22.8	32.7	21.1	13.2	16.3	10.1	12.2	15.1	16.9	13.2	18.1
$Kp = P_{CO2}P_{H2}/P_{CO}/P_{H2O}$	3.20	0.85	2.58	0.96	0.48	0.61	0.39	0.40	0.59	0.61	0.50	0.65
HC selectivity (wt.%)[c]												
CH_4	22.3	23.6	22.9	23.0	25.3	24.5	24.4	25.0	16.3	18.1	15.6	16.9
C_2–C_4	49.6	44.5	50.1	46.3	46.8	45.4	46.5	45.7	39.6	42.7	39.2	41.1
C_5^+	28.1	31.9	27.0	30.7	27.9	30.1	29.1	29.3	44.1	39.2	45.2	42.0
$C_{2-4}^=/C_{2-4}^0$	0.42	0.40	0.36	0.36	0.30	0.32	0.31	0.32	0.51	0.49	0.50	0.48
$C_{5-11}^=/C_{5-11}^0$	0.44	0.43	0.45	0.42	0.41	0.41	0.40	0.40	0.48	0.46	0.45	0.44

[a] Reaction conditions: 280 °C, 1.5 MPa, H_2/CO = 2.0, 2 NL/(g of catalyst·h), and TOS of ca. 200 h.
[b] TOF: turnover frequencies for CO conversion, i.e., the number of CO molecules converted per surface catalytic site (based on H_2 uptake) per second under present FTS reaction conditions.
[c] HC: Hydrocarbon.

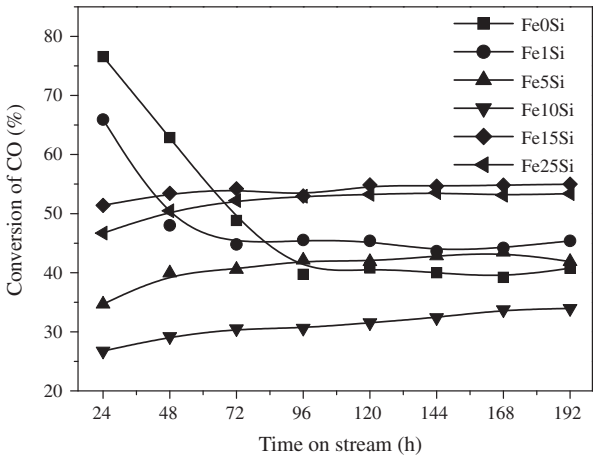

Fig. 9. Carbon monoxide conversion with time on stream for catalysts.

iron and mostly plays a physical role in catalysts. It is evident that the intrinsic role of silica in FTS catalysts is partly hidden by the quite different interactions among Fe–SiO_2 and K–SiO_2 in those multicomponent catalyst systems [6,8,15]. In the present study, the effects of chemical promoters have been ruled out. It is more convenient to elucidate the intrinsic roles of silica in FTS reactions using the binary Fe/SiO_2 model catalysts.

According to the characterization results in the above paragraphs, silica addition significantly affects the physical and chemical properties of catalysts, i.e., a lower reduction degree and a smaller particle size. It is widely suggested that the iron carbide phase is the active phase in FTS [54,55]. The different reduction or carburization extent may explain the variation of the FTS activity with changing silica content and time on stream. As indicated by MES (Table 2), the silica-free catalyst contains the highest iron carbide content among all catalysts after activation. Moreover, the iron carbide in the catalyst was almost reoxidized into iron oxides after reaction. This well explains the high initial activity and the deactivation of the catalyst. Furthermore, iron carbide content can explain the initial activity variation of catalysts with different silica content to some extent. However, there are some exceptions. For example, Fe10Si shows the lowest activity among all catalysts, while it does not contain the lowest iron carbide content either after activation or after reaction. The steady activity of all catalysts cannot be well correlated with the iron carbide content. These exceptions imply that the reduction degree is not the only factor to affect the FTS activity of these Fe/SiO_2 catalysts. The FTS reactions on iron catalysts were reported to be structure-sensitive [56,57]. Boudart and McDonald [56] found that, over iron supported on MgO catalysts, the site–time yield of methane synthesis increased by over one order of magnitude as the iron particle size changed between 1 and 17 nm. Jones et al. [18] found that, over iron supported on carbon catalysts, the initial CO TOF increased by a factor of 40 as the crystallite size increased from <1.2 to 7.9 nm. In the present study, the initial FTS activity follows a similar tendency between small and large iron particles. It is indicated that the iron particle size has an apparent effect on the FTS activity. It should be noted that the FTS activity does not show a monotonic increasing tendency as the crystallite size increases over the Fe/SiO_2 catalysts. This could be due to double effects of the reduction degree and the structure sensitivity. All in all, silica affects the FTS activity of iron catalysts in two ways: (1) a decreased reduction degree and (2) a decreased crystallite size.

3.6.2. Product selectivity

The methane and high-molecular-weight hydrocarbon (C_5^+) selectivities of catalysts with TOS are shown in Fig. 10. Detailed

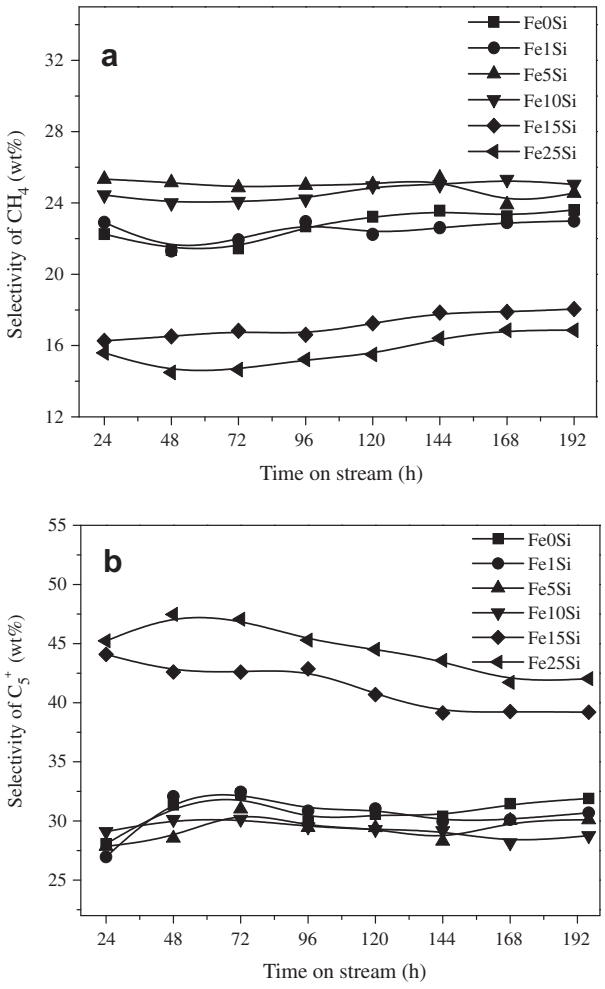

Fig. 10. (a) CH_4 and (b) C_5^+ selectivity with time on stream for catalysts.

hydrocarbon distributions at the beginning and the end of the reaction (24 and 192 h) are summarized in Table 5. For Fe0Si and Fe1Si, hydrocarbon distributions are nearly identical. In comparison with Fe0Si, Fe5Si and Fe10Si slightly shift the hydrocarbon product to methane and decrease the C_5^+ hydrocarbon selectivities. With further increasing silica content, Fe15Si and Fe25Si remarkably suppress the selectivity to methane but enhance the selectivities to C_5^+ hydrocarbons. In Table 5, olefin/paraffin ratios also show a tendency to first decrease, reach a minimum at Fe10Si, and then increase remarkably with increasing silica content. In addition, the hydrocarbon distribution and olefin/paraffin ratios are nearly constant in the whole TOS for each catalyst; i.e., the hydrocarbon distribution is nearly independent of the variation of iron carbide content in the reaction. Bukur et al. [6] also reported the effect of the silica content on FTS product selectivities over 100Fe/5Cu/4.2 K/$x$$SiO_2$ catalysts. They found that high-molecular-weight hydrocarbon and olefin selectivities increased with increasing silica content, except for the catalyst containing 24SiO_2/100Fe. They did not observe a parabolic trend of hydrocarbon selectivities in this work. Yang et al. [15] observed a first increase and later decrease in the methane selectivity as the silica content increased over FeMnK/SiO_2 catalysts. They thought this trend was unexpected from the point of view of the effective potassium content. In fact, these results are generally in agreement with the results in the present work. The presence of potassium has slightly affected the judgments of the intrinsic effect of silica.

Silica is well known to be inert for CO hydrogenation reactions. How does silica change the FTS selectivity of iron catalysts? On one

hand, silica apparently affects the reduction behavior of iron catalysts. Poor reduction behavior would lead to a lower active phase content and lower CO conversion. It is reported that the CO conversion level can also affect the product selectivity [58]. Actually, the CO conversion level changes the H_2/CO ratio in the reactor. A high H_2/CO ratio can facilitate the methane production. However, as shown in Table 5, the exit H_2/CO ratios fall in ranges of 2.1–2.5 for all catalysts at different reaction stages. There is no direct correlation of the CO conversion level and the exit H_2/CO ratio with the hydrocarbon selectivity. For example, Fe10Si has the lowest CO conversion and the lowest exit H_2/CO ratio among all catalysts, while it exhibits higher methane selectivity. In addition, the CO conversion of Fe0Si catalyst quickly decreases from about 70 to 40%, while the methane selectivity slightly increases during the whole reaction. These results indicate that the H_2/CO ratio or CO conversion level has a negligible influence on the product selectivity in the Fe/SiO_2 catalysts. In contrast, there is some relationship between the reduction degree and the product selectivity. For example, the iron oxide content increases after activation with increasing silica content. Coincidentally, CH_4 and paraffin selectivities slightly increase with increasing silica content, except for Fe15Si and Fe25Si catalysts. It seems that the low reduction extent slightly increases light hydrocarbon and paraffin selectivities. On the other hand, silica has important influences on the structure of the active phase. Generally, active phases have important influences on the product selectivity of an FTS reaction [59]. Although MES results indicate no intrinsic difference in iron carbide structures of catalysts, XRD, TEM, and H_2 TPD confirm that silica decreases the iron crystallite size and improves the proportion of deep hollow or defect sites of surface iron atoms. CO-TPD results have confirmed that C and O adsorption is strengthened on catalysts with small iron particles or high silica content (Fe15Si and Fe25Si). The strengthened surface Fe–C probably piles up the reaction barrier of surface carbon hydrogenation. McDonald et al. [57] found that large Fe particles produced a lower fraction of C_2^+ in the hydrocarbon product over Fe/MgO catalysts. In the present study, Fe/SiO_2 catalysts show similar trends for hydrocarbon selectivity with changing iron crystallite size, except for the hardly reducible catalysts (Fe5Si and Fe10Si). From these results, it is obvious that the crystallite size has an important effect on the hydrocarbon selectivity. Comparing the two factors, the structure of the active phase is more important than the reduction extent in determining the selectivity of Fe/SiO_2 catalysts.

3.7. Roles of silica in catalysts

Silica is usually considered to influence the physical properties of a catalyst but not the chemical features. However, this work provides considerable evidence to show that silica impacts not only the physical properties but also the chemical characteristics of iron catalysts.

The foregoing H_2 TPR and MES results indicate that the added silica significantly restrains the reduction and carburization of catalysts. FT-IR results show the formation of Fe—O—Si structure in as-prepared catalysts. Moreover, the Fe_2SiO_4 phase was observed during FTS reaction of high-silica-content catalysts. According to the XPS results, the electron transfer results in an electron-deficient state of Fe. Thus, more electron density of Fe nuclei takes part in Fe–O covalent bonds, leading to the strengthening of the Fe–O bonds. As a result, oxygen removal in iron oxides during reduction or activation becomes difficult. Therefore, the SiO_2-promoted catalysts exhibit a lower degree of reduction and carburization. Oxygen can be expected to withdraw electrons from the less electronegative iron surface and weaken the chemisorption of CO and H_2, especially for CO dissociation [48,60]. Thus, the hardly removable oxygen species plays a crucial role in inhibiting the reduction of hardly reducible Fe/SiO_2 catalysts (e.g., Fe5Si and Fe10Si) and in determining the catalytic activities and selectivities.

SiO_2 also has an important structural effect on the iron species in catalysts. N_2 physisorption results (Table 1) indicate that silica incorporated into the iron catalysts increases the BET surface area of the catalysts. Moreover, XRD and TEM results show that the average crystalline size of iron oxide in catalysts progressively decreases with increasing silica content. The nanosize states of iron particles are preserved during activation and FTS reaction. MES results also indicate that the highly dispersed catalysts can continuously generate and stabilize the χ-Fe_5C_2 species during the reaction process. In highly dispersed catalysts, the iron particle size probably becomes an important factor in the activity of the catalysts. These nanoparticles can provide more surface atoms and a larger number of adsorption sites for CO and H_2 [61]. Therefore, it is reasonable that the steady-state FTS activity increases on the highly dispersed catalysts (Fe15Si and Fe25Si). In addition, the particle size of iron carbide has an important influence on the product selectivity. It is well known that nanoparticles have higher surface energy [30,62]. Most importantly, nanoparticles have more surface atoms and a higher concentration of highly coordinated unsaturated sites (defect, edge, and corner atoms). These undercoordinated atoms have different electron structures relative to those at crystal faces [63] and finally affect H_2 and CO chemisorption on catalysts (as proved by H_2-TPD and CO-TPD). With strengthening of the surface carbon adsorption, the highly dispersed catalysts show higher C_5^+ and lower methane selectivities in the FTS reactions.

4. Conclusions

In this study, Fe–SiO_2 interaction and its effect on chemical/structural properties and catalytic performance of Fe/SiO_2 catalysts were studied. The Fe—O—Si bond was observed in SiO_2-promoted catalysts, which changed the electronic structures of iron atoms. Moreover, a fayalite (Fe_2SiO_4) phase was observed in Fe25Si catalysts after the FTS reaction. The addition of silica increases the BET surface area of catalysts and decreases the iron particle size. Also, the SiO_2 species are beneficial for stabilizing the crystallite sizes and the active phases during the FTS reaction. In reduction or activation, a small amount of silica inhibits the reduction or carburization of catalysts, while a large amount of silica improves the reduction or carburization of iron oxides not directly bonding with silica. Silica has a great influence on H_2 and CO chemisorption of catalysts. A small amount of silica can increase H_2 uptake on reduced catalysts. A large amount of silica can greatly decrease the amount of weakly adsorbed H species but enhance the amount of strongly adsorbed H species. Silica also strengthens the adsorption of C and O on carburized catalyst surfaces from CO-TPD results.

In FTS reactions, silica has multiple effects on catalytic performances of catalysts. First, silica improves the stability of catalysts. Second, the FTS activity first decreases, passes a minimum at Fe10Si, and then sharply increases with increasing silica content in catalysts. Third, the selectivity to methane is greatly decreased on high-silica-content catalysts (Fe15Si and Fe25Si). This catalytic behavior can be explained by chemical and structural effects of silica on iron oxides/carbides.

Acknowledgments

We thank the National High Technology Research and Development Program of China (2011AA05A205), the National Natural Science Foundation of China (21173249) and Chinese Academy of

Sciences Knowledge Innovation Project (KJCX2-YW-N41). This work is also supported by Synfuels CHINA. Co., Ltd.

Appendix A. Supplementary material

Supplementary data associated with this article can be found, in the online version, at doi:10.1016/j.jcat.2011.10.024.

References

[1] M.E. Dry, Appl. Catal. A Gen. 276 (2004) 1.
[2] D.S. Kalakkad, M.D. Shroff, S. Köhler, N. Jackson, A.K. Datye, Appl. Catal. A Gen. 133 (1995) 335.
[3] K.K. Liu, H.Y. Suo, C.H. Zhang, J. Xu, Y. Yang, H.W. Xiang, Y.W. Li, Catal. Commun. 12 (2010) 137.
[4] E. de Smit, B.M. Weckhuysen, Chem. Soc. Rev. 37 (2008) 2758.
[5] R. Zhao, J.G. Goodwin Jr., K. Jothimurugesan, S.K. Gangwal, J.J. Spivey, Ind. Eng. Chem. Res. 40 (2001) 1065.
[6] D.B. Bukur, X. Lang, D. Mukesh, W.H. Zimmerman, M.P. Rosynek, C. Li, Ind. Eng. Chem. Res. 29 (1990) 1588.
[7] H.J. Wan, B.S. Wu, C.H. Zhang, H.W. Xiang, Y.W. Li, B.F. Xu, F. Yi, Catal. Commun. 8 (2007) 1538.
[8] N. Egiebor, W.C. Cooper, Can. J. Chem. Eng. 63 (1985) 81.
[9] M.E. Dry, Catal. Sci. Technol. 1 (1981) 159.
[10] P.K. Basu, S.B. Basu, S.K. Mitra, S.S. Dasandhi, S.S. Bhattcherjee, P. Samuel, Stud. Surf. Sci. Catal. 113 (1998) 277.
[11] C.R.F. Lund, J.A. Dumesic, J. Phys. Chem. 85 (1981) 3175.
[12] A.F.H. Wielers, A.J.H.M. Kock, C.E.C.A. Hop, J.W. Geus, A.M. van der Kraan, J. Catal. 117 (1989) 1.
[13] H. Dlamini, T. Motjope, G. Joorst, G. ter Stege, M. Mdleleni, Catal. Lett. 78 (2002) 201.
[14] C.H. Zhang, H.J. Wan, Y. Yang, H.W. Xiang, Y.W. Li, Catal. Commun. 7 (2006) 733.
[15] Y. Yang, H.W. Xiang, L. Tian, H. Wang, C.H. Zhang, Z.C. Tao, Y.Y. Xu, B. Zhong, Y.W. Li, Appl. Catal. A Gen. 284 (2005) 105.
[16] H.J. Wan, B.S. Wu, Z.C. Tao, T.Z. Li, X. An, H.W. Xiang, Y.W. Li, J. Mol. Catal. A 260 (2006) 255.
[17] C.H. Zhang, Y. Yang, B.T. Teng, T.Z. Li, H.Y. Zheng, H.W. Xiang, Y.W. Li, J. Catal. 237 (2006) 405.
[18] V.K. Jones, L.R. Neubauer, C.H. Bartholomew, J. Phys. Chem. 90 (1986) 4832.
[19] Y.Y. Ji, H.W. Xiang, J.L. Yang, Y.Y. Xu, Y.W. Li, B. Zhong, Appl. Catal. A Gen. 214 (2001) 77.
[20] S.M. Rodulfo-Baechler, S.L. Gonzalez-Cortes, J. Orozco, V. Sagredo, B. Fontal, A.J. Mora, G. Delgado, Mater. Lett. 58 (2004) 2447.
[21] S. Bruni, F. Cariati, M. Casu, A. Lai, A. Musinu, G. Piccaluga, S. Solinas, Nanostruct. Mater. 11 (1999) 573.
[22] P. Fabrizioli, T. Bürgi, M. Burgener, S. van Doorslaerb, A. Baiker, J. Mater. Chem. 12 (2002) 619.
[23] S. Bordiga, R. Buzzoni, F. Geobaldo, C. Lamberti, E. Giamello, A. Zecchina, G. Leofanti, G. Petrini, G. Tozzola, G. Vlaic, J. Catal. 158 (1996) 486.
[24] J.M. Zhao, Z. Feng, F.E. Huggins, G.P. Huffman, Energy Fuels 8 (1994) 38.
[25] M. Qing, Y. Yang, B.S. Wu, J. Xu, C.H. Zhang, P. Gao, Y.W. Li, J. Catal. 279 (2011) 111.
[26] T. Yamashita, P. Hayes, Appl. Surf. Sci. 254 (2008) 2441.
[27] W.E. Kaden, T. Wu, W.A. Kunkel, S.L. Anderson, Science 326 (2009) 826.
[28] S.D. Qin, C.H. Zhang, J. Xu, H.W. Xiang, Y.W. Li, Appl. Catal. A Gen. 392 (2011) 118.
[29] F.J. Berry, S. Skinner, M.F. Thomas, J. Phys. Condens. Matter. 10 (1998) 215.
[30] F.X. Redl, C.T. Black, G.C. Papaefthymiou, R.L. Sandstrom, M. Yin, H. Zeng, C.B. Murray, S.P. O'Brien, J. Am. Chem. Soc. 126 (2004) 14583.
[31] J.F. Bengoa, A.M. Alvarez, M.V. Cagnoli, N.G. Gallegos, S.G. Marchetti, Appl. Catal. A Gen. 325 (2007) 68.
[32] S.C. Lin, J. Phillips, J. Appl. Phys. 58 (1985) 1943.
[33] S.S. Hafner, J. Stanek, M. Stanek, J. Phys. Chem. Solids 51 (1990) 203.
[34] M.E. Dry, Catal. Lett. 7 (1990) 241.
[35] W.S. Ning, N. Koizumi, H. Chang, T. Mochizuki, T. Itoh, M. Yamada, Appl. Catal. A Gen. 312 (2006) 35.
[36] N. Sirimanothan, H.H. Hamdeh, Y. Zhang, B.H. Davis, Catal. Lett. 82 (2002) 181.
[37] F. Arena, G. Gatti, G. Martra, S. Coluccia, L. Stievano, L. Spadaro, P. Famulari, A. Parmaliana, J. Catal. 231 (2005) 365.
[38] F. Bozso, G. Ertl, M. Grunze, M. Weiss, Appl. Surf. Sci. 1 (1977) 103.
[39] K. Yashida, G.A. Somorjai, Surf. Sci. 75 (1978) 46.
[40] P.B. Merrill, R.J. Madix, Surf. Sci. 347 (1996) 249.
[41] G. Wedler, D. Borgmann, Ber. Bunsenges. Phys. Chem. 78 (1974) 67.
[42] G.D. Weatherbee, J.L. Rankin, C.H. Bartholomew, Appl. Catal. 11 (1984) 73.
[43] S.P. Walch, Surf. Sci. 143 (1984) 188.
[44] W. Moritz, R. Lmbihl, R.J. Behm, G. Ertl, T. Matsushima, J. Chem. Phys. 83 (1985) 1959.
[45] S.L. Bernasek, M. Zappone, P. Jiang, Surf. Sci. 272 (1992) 53.
[46] G.C. Bond, Stud. Surf. Sci. Catal. 17 (1983) 285.
[47] F. Benseradj, F. Sadi, M. Chater, Appl. Catal. A Gen. 228 (2002) 135.
[48] J.B. Benziger, R.J. Madix, Surf. Sci. 94 (1980) 119.
[49] U. Seip, M.C. Tsai, K. Christmann, J. Kippers, G. Ertl, Surf. Sci. 139 (1984) 29.
[50] J.B. Benziger, R.J. Radix, Surf. Sci. 115 (1982) 279.
[51] G. Blyholder, M. Lawless, Langmuir 7 (1991) 140.
[52] C.F. Huo, J. Ren, Y.W. Li, J.G. Wang, H.J. Jiao, J. Catal. 249 (2007) 174.
[53] Z.Y. Ma, C.F. Huo, X.Y. Liao, Y.W. Li, J.G. Wang, H.J. Jiao, J. Phys. Chem. C 111 (2007) 4305.
[54] T. Riedel, H. Schulz, G. Schaub, K.-W. Jun, J.-S. Hwang, K.-W. Lee, Top Catal. 26 (2003) 41.
[55] L.D. Mansker, Y. Jin, D.B. Bukur, A.K. Datye, Appl. Catal. A Gen. 186 (1999) 277.
[56] M. Boudart, M.A. McDonald, J. Phys. Chem. 88 (1984) 2158.
[57] M.A. McDonald, D.A. Storm, M. Boudart, J. Catal. 102 (1986) 386.
[58] B.H. Davis, Ind. Eng. Chem. Res. 46 (2007) 8938.
[59] C.-F. Huo, Y.-W. Li, J.-G. Wang, H.-J. Jiao, J. Am. Chem. Soc. 131 (2009) 14713.
[60] T.J. Vink, L.L.J. Gijzeman, J.W. Geus, Surf. Sci. 150 (1985) 4.
[61] K.J. Klabunde, J. Stark, O. Koper, C. Mohs, D.G. Park, S. Decker, Y. Jiang, I. Lagadic, D. Zhang, J. Phys. Chem. 100 (1996) 12142.
[62] X.B. Chen, Y.C. Li, P.D. Hodgson, C. Wen, Acta Biomater. 5 (2009) 2290.
[63] G. Blyholder, J. Phys. Chem. 68 (1964) 2772.